

Quantification of STEM-in-SEM Energy Dispersive X-ray Spectra using Bulk Standards

Nicholas W. M. Ritchie^{(1)*}(ORCID: 0000-0001-5734-5729)

Andrew Herzing⁽¹⁾ (ORCID: 0000-0001-5944-2610)

Vladimir P. Oleshko⁽¹⁾ (ORCID: 0000-0003-0538-2354)

⁽¹⁾National Institute of Standards and Technology
Gaithersburg, MD 20899

February 2, 2024

Abstract

A quantification model which uses standard X-ray spectra collected from bulk materials to determine the composition and mass-thickness of single-layer and multi-layer unsupported thin-films is presented. The multi-variate model can be iteratively solved for single layers in which each element produces at least one visible characteristic X-ray line. The model can be extended to multi-layer thin films in which each element is associated with only one layer. The model may sometimes be solved when an element is present in multiple layers if additional information is added in the form of independent k-ratios or model assumptions. While the algorithm is suitable for any measured k-ratios, it is particularly well suited to energy-dispersive X-ray spectrometry (EDS) where the bulk standard spectra can be used to deconvolve peak interferences in the thin-film spectra. The algorithm has been implemented and made available in the Open Source application NIST DTSA-II. We present experimental data and Monte Carlo simulations supporting the quantification model.

Keywords: Quantitative electron-excited X-ray microanalysis, energy-dispersive spectrometry (EDS), STEM-in-SEM, NIST DTSA-II software, bulk standards, thin films, thickness

1 Introduction

The first energy dispersive X-ray spectrometers (EDS) installed on a electron micro-probe were introduced in 1968(Fitzgerald et al., 1968). Soon thereafter, EDS detectors were installed on transmission electron microscopes (TEM) and scanning TEMs (STEM), and attempts were made to quantify the X-ray spectra collected on these instruments. An early successful attempt, that remains popular, is that of Cliff and Lorimer(Cliff & Lorimer, 1975). TEMs are typically high voltage instruments (>80 kV) in which the sample is thin enough to be effectively transparent to the incident electron beam. Placing a bulk sample in the beam would block the fluorescence screen used to image the sample and at these energies, it is hard to keep backscattered electrons from striking the X-ray detector. As a result, the Cliff and Lorimer algorithm is based on the comparison of thin film samples to thin film standards. Furthermore, it was often difficult to measure the incident probe current or the thickness of the standard or unknown sample. As a result, the technique resorted to comparing the relative amplitudes of characteristic X-ray peaks from elements present in both the standard and unknown. This ratio would be a function of only the relative mass-fraction of the elements in the standard and unknown. In the absence of absorption and X-ray fluorescence, the defining expression for the Cliff-Lorimer correction is

*Corresponding author: Nicholas W. M. Ritchie, E-mail: <mailto:nicholas.ritchie@nist.gov>

Variable	Definition	Notes
Z	Atomic Number	Specifies the element
C_Z	Mass fraction of element Z	(g g^{-1})
k_{CL}	Cliff-Lorimer factor	Unique to a pair of elements and conditions (dimensionless)
l	Sub-shell index	Specifies the atomic sub-shell within an element Z
j	Transition index	Specifies a characteristic X-ray transition resulting from ionization in sub-shell l
I_j	X-ray intensity	Characteristic X-ray intensity for the j -th transition (Counts)
ρ	Density	Density of the bulk or film constituent material (g/cm^3)
t	Film thickness	(cm)
$\phi(\rho z)$	Ionization depth profile	Ionization depth profile for the l -th sub-shell
ω_j	Fluorescence yield	Probability of an ionization of the l sub-shell relaxing via a j characteristic X-ray
E_0	Incident beam energy	Electron kinetic energy for the incident beam (keV)
$Q_l^Z(E_0)$	Ionization cross-section	The ionization cross-section for the l -shell of the A -atom for electrons of kinetic energy E_0 .
A_Z	Atomic weight	Atomic weight of the element Z (g)
E_l	Critical excitation energy	Energy required to ionize the l shell (keV)
J_Z	Mean ionization potential	Inelastic energy loss term in the Bethe model (eV)
R_Z	Backscatter Factor	The backscattered factor for the element Z (dimensionless)
Ω	Detector solid angle	Maintained between thin-film and bulk measurements (sr)
ϵ_j	Fractional detector efficiency for j -line	By using the sample characteristic line, this term cancels.
$\iota\tau$	Probe dose	Product of the probe current and acquisition live time (nAs)
q_{e^-}	Electron charge	Physical constant (C)
N	Avogadro's Number	(atoms/mol)
F	Secondary fluorescence correction	Reed or similar bulk fluorescence correction
$k_{j,\mathbb{F},\mathbb{B}}$	k-ratio	The ratio of the dose-normalized X-ray intensities measured on the thin-film and standard for the j transition.
χ	Extended mass-absorption coefficient	$\chi = \left[\frac{\mu}{\rho}\right]_j \csc(\theta)$ where $\left[\frac{\mu}{\rho}\right]_j$ is the material mass-absorption coefficient (cm^2/g) for the transition j and θ is the take-off angle.

Table 1: Definition of the model parameters used in this paper. Variables may be further distinguished by the sub-scripts \mathbb{F} and \mathbb{B} corresponding to the film and bulk, respectively.

$$\frac{I_{j_1}}{I_{j_2}} = \frac{C_{Z_1}}{C_{Z_2}} k_{CL} \quad (1)$$

where the variables are defined in Table 1 and the indices 1 and 2 represent two elements present within the film and k_{CL} is determined from a thin-film standard containing these two elements. Even when a standard is not available for exactly the elements present in the unknown, it is common to develop an instrument-specific calibration curve that can be interpolated to provide k_{CL} factors for unavailable elements. If elemental ratios are measured for all elements in a sample, the elemental ratios can be converted into absolute mass fractions through normalization. It is not possible to measure the mass-thickness using the Cliff-Lorimer technique.

The Cliff-Lorimer correction proved useful but requires multi-element thin films of known composition for use as standards. In response, the National Institute of Standards and Technology (NIST) released in 1987 a multi-element thin film standard made from a Mg/Si/Ca/Fe oxide glass called Standard Reference Material (SRM) 2063. It proved popular and, when the original supply ran out, it was reissued in 1993 as SRM-2063a. The certified composition of SRM-2063a was 0.0797(34) Mg, 0.2534(98) Si, 0.1182(37) Ca, 0.1106(88) Fe and 0.432(16) O by mass-fraction. SRM 2063a consisted of a mineral glass film deposited onto a 20 nm-thick carbon support film on a 3 mm diameter copper microscopy grid. The density and thickness were not certified but information values of 3.1(3) g/cm³ and 76(4) nm were provided and correspond to an uncertainty of 10 % in the mass-thickness.

The ζ -factor method of Watanabe and Williams (Watanabe & Williams, 2006) represented an advance on the Cliff-Lorimer method. The ζ -factor method requires thin-film standards of either pure elements or known compounds with known mass-thickness. Pure-element thin films are easier to produce and characterize than multi-element thin films because the composition and density of multi-element thin-films can be hard to establish. While it is not possible to construct thin films from all elements, it is possible to construct them from a large fraction of the periodic table and intermediate elements can be interpolated. While Cliff-Lorimer is a ratio-based technique, the ζ -factor method measures the absolute amount of an element in a sample which can be used to estimate both the mass fraction and mass-thickness of the unknown sample. In the ζ -factor method, the standard serves to measure a quantity that is proportional to the ionization cross-section and is a function of the geometry and efficiency of the EDS detector. While there are many advantages to the ζ -factor method, it still requires standards of a form that can be a challenge to produce and characterize with the desired accuracy. MacArthur (MacArthur et al., 2016) and Varambhia (Varambhia et al., 2018) re-expressed the ζ -factor method in terms of partial cross-sections.

A recent article by Parisini *et al* (Parisini et al., 2018) presents a comparison of these techniques using modern instrumentation and applied to simple problems of technological interest. The Cliff-Lorimer and ζ -factors remain the preferred algorithms for quantification in the S/TEM.

Before Cliff-Lorimer, an alternative scheme that employed bulk standards for X-ray microanalysis of thin films was studied by several researchers (Duncumb, 1968; Philibert & Tixier, 1968; Nasir, 1972; Jacobs & Baborovska, 1972; Jacobs, 1973). In one of the first studies (Sweeney Jr et al., 1960), Sweeney proposed to calculate the ratio of the X-ray intensity measured on a thin film $I_{j_{\mathbb{F}}}$ for element Z to the intensity measured on a bulk standard of the same element, $I_{j_{\mathbb{B}}}$, according to the following equation:

$$\frac{I_{j_{\mathbb{F}}}}{I_{j_{\mathbb{B}}}} = \frac{C_{Z_{\mathbb{F}}} \int_0^{\rho_{\mathbb{F}} t} \phi_{\mathbb{F}}(\rho z) \exp(-\chi_{\mathbb{F}} \rho z) d\rho z}{\int_0^{\infty} \phi_{\mathbb{B}}(\rho z) \exp(-\chi_{\mathbb{B}} \rho z) d\rho z} \quad (2)$$

where the parameters are described in Table 1. For unsupported 50 nm-thick gold films and bulk gold, $\phi_{\mathbb{B}}(\rho z)$ and $\phi_{\mathbb{F}}(\rho z)$ profiles were calculated using Monte Carlo simulations and then converted into the intensity ratios, demonstrating the agreement between experimental and theoretically calculated values within 10 % (Bolon et al., 1975). In the bulk standard approach, thin film specimen intensities were calculated by simply assuming the electron trajectory is the same as the specimen thickness t :

$$I_{j_{\mathbb{F}}} = \text{const} \cdot C_Z \omega_j Q_i^A(E_0) t/A_Z \quad (3)$$

where the parameters are described in Table 1. In this case, the bulk standard intensity can be calculated using a ZAF correction (Goldstein, 1979). For two elements Z_1 and Z_2 in an unsupported thin film when fluorescence and absorption effects are assumed to be negligible, the ratio of corrected intensities is given by (Bolon et al., 1975; Goldstein, 1979):

$$\frac{I_{Z_1\mathbb{F}}/I_{Z_1\mathbb{B}}}{I_{Z_2\mathbb{F}}/I_{Z_2\mathbb{B}}} = \frac{C_{Z_1} P_{Z_1}}{C_{Z_2} P_{Z_2}}, \quad (4)$$

where the correction factors are defined by

$$P_{Z_i} = \frac{\log(U_{l_i})}{E_{l_i} R_{Z_i} / S_{Z_i}}, \quad (5)$$

$$\frac{1}{S_{Z_i}} = \int_1^{U_{l_i}} \frac{\log(U) dU}{M_{Z_i} \log(UW_{Z_i})}, \quad (6)$$

$$M_{Z_i} = Z_{Z_i} / A_{Z_i}, \quad (7)$$

$$U_{l_i} = E_0 / E_{l_i}, \quad \text{and} \quad (8)$$

$$W_{Z_i} = 1.166 E_{l_i} / J_{Z_i} \quad (9)$$

for $i = 1$ or 2 . By applying ZAF correction procedures developed for low operating potentials of 15 kV to 35 kV, Duncumb (Duncumb, 1968), demonstrated good results with the EMMA electron microscope-microanalyzer measuring the standard intensities $I_{Z_i\mathbb{B}}$ at low voltages. Jacobs and Baborovska (Jacobs & Baborovska, 1972; Jacobs, 1973), utilized this method successfully with the EMMA-3 operating at accelerating voltages of 100 kV or 40 kV on Al-Fe intermetallic phases, mixed (Ti, Mo)C metal carbides, and MnCr₂O₄ and MgAl₂O₄ spinels in several metallurgical samples.

A few years later (Yakowitz & Newbury, 1976) developed a novel technique for quantifying thin-films on substrates using bulk standards. The method is based on the $\phi(\rho z)$ -curve but developed at a time when analytical expressions for this curve were first being developed. As a result it relies heavily on Monte Carlo simulations to compute the $\phi(\rho z)$ -curve. In a section entitled “Compositional Analysis of Thin Film Specimens”, the authors address unsupported thin films. They develop a method to estimate the thickness of the sample.

Later, Dijkstra *et al* (Dijkstra et al., 1994) attempted to address the compositional and thickness quantification of unsupported thin-films using a $\phi(\rho z)$ -method. They based their technique on an established technique for analyses of a thin-film on a substrate but consider the limit in which the atomic number of the substrate goes to zero. This approach was further developed for using in a TEM (Boon, 2000; Boon & Bastin, 2000, 2004). A similar but less sophisticated version of this approach was implemented by Lang (Lang et al., 2014) using Oxford’s AZtec LayerProbe¹ assuming a low-Z substrate to quantify unsupported thin films. This approach which builds on supported thin film algorithms is likely to support thick samples at low beam energies better than the simple algorithm presented herein. Dijkstra (Dijkstra et al., 1994) shows an example at 10 keV where the film is approximately 1/3 the thickness of the bulk excitation depth. Like the technique in this paper, these techniques can estimate both the composition and the mass-thickness of the sample.

A US Patent (Statham, 2018) suggests that the mass-thickness of a unsupported thin-film can be determined by comparison with a calibrated thin-film of known mass-thickness and composition. Statham (Statham et al., 2018) also presents a method for using a single SiN standard of uniform thickness (100 nm) to calibrate the electron dose and detector solid angle. They then proposes to use these calibrated values to calculate the mass fraction and thickness using the ionization cross-section, the fractional yield and the detector efficiency. The method herein eliminates the need for these poorly-known theoretical values by replacing them with measured values.

In recent years, there has been an increased interest in microanalysis using STEM-modes in an SEM. Rather than working at the 80 kV to 300 kV accelerating voltages that are typical of the TEM, STEM-in-SEM, as it is known, is commonly performed at the upper-end of the SEM accelerating voltage range (20 kV to 30 kV). This opens up a new opportunity since, while it is generally not practical to collect spectra from bulk materials in a TEM, it is routine in an SEM. Furthermore, bulk materials are readily available with known compositions in ideal geometries. If they are not available in the laboratory, they can be easily purchased from microscopy supply vendors. Bulk materials of known compositions are routinely used to quantify spectra from bulk samples (Newbury & Ritchie, 2015) and thin-films on substrates (Moy & Fournelle, 2020).

¹Any mention of commercial products is for information only; it does not imply recommendation or endorsement by NIST.

This paper revisits the idea of using bulk standards for thin films and presents a novel method that uses analytical $\phi(\rho z)$ -curves proven for bulk analysis to facilitate the use of bulk standards to measure the composition and thickness of unsupported thin films. The technique takes advantage of the characteristic X-ray peak shape present in the bulk spectra to deconvolve the spectrum from the unsupported thin-film. This permits high precision measurement even from elements with highly interfering characteristic line structures. We hope that because it is so much easier to find suitable standards and to collect spectra from bulk materials that this quantification technique might encourage more people to characterize thin-film samples using STEM-in-SEM. Alternatively, multi-element thin films can be characterized using STEM-in-SEM and then applied as standards for S(TEM).

2 Theory

The preferred modern analytical technique for modeling X-ray generation by an electron-beam from a bulk sample are the, so called, $\phi(\rho z)$ models. The intensity of measured X-rays can be calculated using the expression

$$I_{\mathbb{B}} = \left(\frac{\Omega}{4\pi} \right) \epsilon_j \omega_j \left(\frac{[\nu\tau]_{\mathbb{B}}}{q_{e^-}} \right) \left(\frac{C_{Z_{\mathbb{B}}} N}{A_Z} \right) Q_l^Z(E_0) F F_{\chi} \quad (10)$$

where the variables are defined in Table 1, and F_{χ} is defined as

$$F_{\chi} = \int_0^{\infty} \phi_{\mathbb{B}}(\rho z) \exp(-\chi_{\mathbb{B}} \rho z) d\rho z. \quad (11)$$

We used the simplified expression of Pouchou and Pichoir (“XPP”) to implement $\phi(\rho z)$ but other $\phi(\rho z)$ -models may be suitable (Pouchou & Pichoir, 1991).

The expression to describe the generation of X-rays from a very thin film is similar. Essentially, we are using Castaing’s original definition of the $\phi(\rho z)$ -curve (Castaing, 1951) in which the curve’s magnitude is expressed relative to the number of ionizations in an infinitesimally thin film. Thus the equivalent of the $\phi(\rho z)$ -curve for an ultra-thin film is simply the constant unity. We will extend this definition from an infinitesimally thin film to a sufficiently thin-film. So long as we can neglect electron scattering (including backscatter) and energy loss in the incident electron, we can assume the constant unity.

The measured emitted intensity from an unsupported thin-film is

$$I_{\mathbb{F}} = \left(\frac{\Omega}{4\pi} \right) \epsilon_j \omega_j \left(\frac{[\nu\tau]_{\mathbb{F}}}{q_{e^-}} \right) \left(\frac{C_{Z_{\mathbb{F}}} N}{A_Z} \right) Q_l^Z(E_0) \int_0^{\rho_{\mathbb{F}} t} \exp(-\chi_{\mathbb{F}} \rho z) d\rho z \quad (12)$$

The k-ratio, $k_{j,\mathbb{F},\mathbb{B}}$, (distinct from the k-factor in the Cliff and Lorimer technique) is defined as the dose-normalized ratio of these two quantities.

$$k_{j,\mathbb{F},\mathbb{B}} = \frac{I_{\mathbb{F}} / ([\nu\tau]_{\mathbb{F}})}{I_{\mathbb{B}} / ([\nu\tau]_{\mathbb{B}})} \quad (13)$$

$$= \frac{\left(\frac{\Omega}{4\pi} \right) \epsilon_j \omega_j \left(\frac{C_{Z_{\mathbb{F}}} N}{A_Z} \right) Q_l^Z(E_0) \int_0^{\rho_{\mathbb{F}} t} \exp(-\chi \rho z) d\rho z}{\left(\frac{\Omega}{4\pi} \right) \epsilon_j \omega_j \left(\frac{C_{Z_{\mathbb{B}}} N}{A_Z} \right) Q_l^Z(E_0) F F_{\chi}} \quad (14)$$

$$= \frac{C_{Z_{\mathbb{F}}} \int_0^{\rho_{\mathbb{F}} t} \exp(-\chi_{\mathbb{F}} \rho z) d\rho z}{C_{Z_{\mathbb{B}}} F F_{\chi}} \quad (15)$$

Here we have chosen to assume that the sample-detector geometry and detector efficiency are the same for the film and bulk. In practical terms, this means that both spectra must be collected on the same instrument or one in which the relative solid angle, probe current and efficiency have been otherwise calibrated and accommodated (Statham et al., 2018). As is the case for standards-based measurements of bulk samples using bulk standards, most of the poorly known physical and geometrical parameters cancel when the standard and unknowns are measured under identical conditions.

If we ignore the effects of absorption in the film, the expression $\int_0^{\rho_{\mathbb{F}} t} \exp(-\chi \rho z) d\rho z$ in Eq. 15 reduces to $\rho_{\mathbb{F}} t$, the mass-thickness of the film. This suggests that a first approximation to Eq. 15 can be expressed as:

Parameter	Definition
$[\rho_{\mathbb{F}}t]_i$	Mass-thickness of layer i
$C_{Z,i\mathbb{F}}$	Mass fraction of element A in layer i
$\chi_{i\mathbb{F}}$	Extended mass absorption coefficient of layer i

Table 2: Additional variables associated with multiple layers

$$k_{j,\mathbb{F},\mathbb{B}} = \frac{C_{Z\mathbb{F}} \rho_{\mathbb{F}}t}{C_{Z\mathbb{B}} F F_{\chi}} \quad (16)$$

If we solve for $C_{Z\mathbb{F}} \rho_{\mathbb{F}}t$, we get

$$C_{Z\mathbb{F}} \rho_{\mathbb{F}}t = k_{j,\mathbb{F},\mathbb{B}} C_{Z\mathbb{B}} F F_{\chi} \quad (17)$$

It is necessary to measure the k-ratio for each element in the thin film. In practice, this precludes measuring samples with light elements, like H and He, which produce no X-rays. Since we measure C_Z for all Z present in the film then

$$\sum_Z C_{Z\mathbb{F}} = 1 \quad \text{and} \quad \sum_Z C_Z \rho_{\mathbb{F}}t = \rho_{\mathbb{F}}t \quad (18)$$

Thus we have our first estimate of $\rho_{\mathbb{F}}t$ in the approximation that there is no absorption in the film. We can refine this estimate by solving the integral representing absorption in the film and pulling out $\rho_{\mathbb{F}}t$.

$$\int_0^{\rho_{\mathbb{F}}t} \exp(-\chi_{\mathbb{F}} \rho z) d\rho z = \rho_{\mathbb{F}}t \left[\frac{1 - \exp(-\chi_{\mathbb{F}} \rho_{\mathbb{F}}t)}{\chi_{\mathbb{F}} \rho_{\mathbb{F}}t} \right] \quad (19)$$

The expression in the square brackets is the absorption correction. When $\chi_{\mathbb{F}} \rho t$ is small, this term approaches unity from below and when it is large, this term approaches zero. We generally work in the regime where $\chi_{\mathbb{F}} \rho t$ is relatively small and the absorption correction is between about 0.5 and 1.0.

Since this expression is hard to solve analytically, we iteratively estimate $\rho_{\mathbb{F}}t$ to generate converging estimates of the mass-thickness and thus also the absorption correction.

$$C_{Z\mathbb{F}} [\rho_{\mathbb{F}}t]_{i+1} = k_{j,\mathbb{F},\mathbb{B}} C_{Z\mathbb{B}} F F_{\chi} \left[\frac{1 - \exp(-\chi_{\mathbb{F}} [\rho_{\mathbb{F}}t]_i)}{\chi_{\mathbb{F}} [\rho_{\mathbb{F}}t]_i} \right] \quad (20)$$

where i represents the iteration index. Typically, Eq. 20 converges to a steady $\rho_{\mathbb{F}}t$ in two or three iterations.

2.1 Extension to Multiple Layers

This treatment can be extended to multiple layers in the following manner. The measured emitted intensity from a sample consisting of k thin-film layers is

$$I_{\mathbb{F}} = \left(\frac{\Omega}{4\pi} \right) \epsilon_j \omega_j \frac{[\tau]_{\mathbb{F}}}{q_{e^-}} \frac{N}{A_Z} Q_l^Z(E_0) \sum_{i=1 \dots n} C_{Z,i\mathbb{F}} \left(\prod_{k=1 \dots i-1} \exp(-\chi_{k\mathbb{F}} [\rho_{\mathbb{F}}t]_k) \right) \left(\int_0^{[\rho_{\mathbb{F}}t]_i} \exp(-\chi_{i\mathbb{F}} \rho z) d\rho z \right) \quad (21)$$

where additional variables corresponding to the layers are defined in Table 2. The sum is over each layer in which $C_{Z,i}$ is non-zero. The integral over $d\rho z$ represents the absorption within the layer i and the product over k represents absorption by the layers between the i layer and the detector.

The model is readily solved assuming that no element is found in more than one layer in which case only one of the $C_{Z,i}$ is non-zero for each Z . The sum in Eq. 21 reduces to a single term representing generation in the layer n and absorption by this layer and the layers between it and the detector.

$$I_{\mathbb{F}} = \left(\frac{\Omega}{4\pi} \right) \epsilon_j \omega_j \frac{[\tau]_{\mathbb{F}}}{q_{e^-}} \frac{N}{A_Z} Q_l^Z(E_0) C_{Z,n\mathbb{F}} \left(\prod_{k=1 \dots i-1} \exp(-\chi_{k\mathbb{F}} [\rho_{\mathbb{F}}t]_k) \right) \left(\int_0^{[\rho_{\mathbb{F}}t]_i} \exp(-\chi_{i\mathbb{F}} \rho z) d\rho z \right) \quad (22)$$

Consider the case of two layers (as shown in Figure 1) by proceeding as we did before to compute the k-ratio by calculating the ratio of the measured intensities. The expression for the k-ratio of an element present only in the second layer is

$$k_{j,\mathbb{F},\mathbb{B}} = \frac{C_{A\mathbb{B}}}{C_{Z,2\mathbb{F}}} \frac{FF_{\chi}}{\chi_{\mathbb{F}2} [\rho_{\mathbb{F}t}]_{2,i} \exp(-\chi_{\mathbb{F}1} [\rho_{\mathbb{F}t}]_1) \frac{1 - \exp(-\chi_{\mathbb{F}2} [\rho_{\mathbb{F}t}]_2)}{\chi_{\mathbb{F}2} [\rho_{\mathbb{F}t}]_{2,i}}}. \quad (23)$$

If there are m distinct elements in layer 1 and n distinct elements in layer 2, then there is typically a minimum of $m + n$ k-ratios and $m + n + 2$ measurands (compositions and thicknesses). By imposing the additional constraint that the total mass-fraction must equal unity in each layer, we end up with $m + n + 2$ constraints for $m + n + 2$ unknowns. If an element is present in two layers, then there are $m + n - 1$ k-ratios but there remain $m + n + 2$ measurands and additional information is required to solve the equations. This information can be in terms of the known composition of a layer, in terms of stoichiometric assumptions, in terms of multiple k-ratios measured on the same element (K's and L's, or L's and M's) or in terms of k-ratios measured at multiple beam energies.

One simple example of a constrained measurement is an oxide layer on a single surface like SiO₂ on Si or Al₂O₃ on Al. Since all the compositions are known, the only unknowns are the thickness of the substrate and the oxide layer. Thus constrained, Eq. 23 is readily solved. When the oxide layer is on both sides, it may be possible to flip the sample and collect data from each direction.

2.2 Limitations

The technique is based on the assumption that $\phi_{\mathbb{F}}(\rho z) = 1$. This assumption degrades as the mass-thickness of the sample increases. The degradation initially results from increased path length as the electron elastically scatters in the thin-film (see Figure 2.) As a result, the degradation leads to mean $\phi_{\mathbb{F}}(\rho z)$ factors that are slightly larger than unity which tends to be similar for all elements (see Figure 3.) The mean $\phi_{\mathbb{F}}(\rho z)$ scales the right-hand side of Eq. 20 similarly for each element which normalizes out in the calculation of composition but leads to an overestimate of the film thickness.

In addition, to the systematic uncertainty associated with underestimating the mean $\phi(\rho z)$ (type B), there are also uncertainties associated with count statistics (type A), mass absorption coefficients (type B), the integral of the bulk $\phi(\rho z)$ model (type B) and the uncertainty in the composition of the standard (type B.) The uncertainty due to count statistics is the easiest to characterize (McCarthy & Schamber, 1981). The uncertainty in the composition of the standard can be vanishingly small for a pure element or stoichiometric compound. Uncertainty in the mass absorption coefficients is discussed elsewhere (Chantler et al., 2005; Ritchie, 2020). Depending on the energy of the X-ray and the proximity to absorption edges, the uncertainty in the mass absorption coefficient may range from less than a percent to fifty percent or more. This uncertainty is less of an issue for thin films in

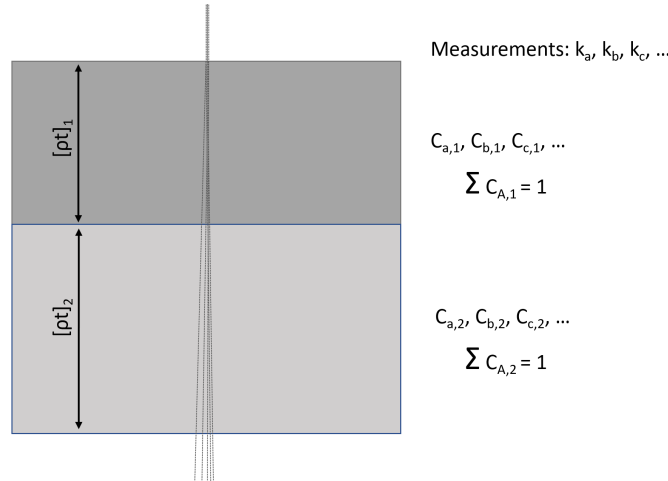


Figure 1: A schematic diagram of a two-layer thin-film sample with the important measures.

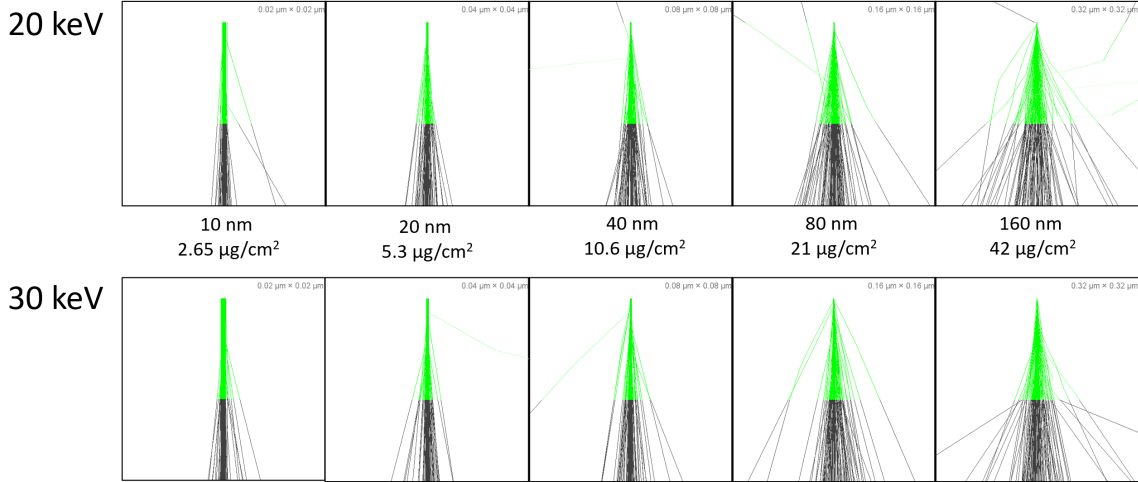


Figure 2: Monte Carlo simulated electron trajectories for a thin film of SiO₂ ($\rho = 2.65 \text{ g/cm}^3$) for incident beam energies of 20 keV (top) and 30 keV (bottom). The green represents the trajectory within the thin film and the black represents the trajectory in the vacuum below the sample. As the sample gets thicker, the width of the exit beam expands leading to an increase in the mean value of the $\phi(\rho z)$. As beam energy increases, the width of the exit beam decreases for a given thickness.

which absorption is typically a minor correction but could hypothetically lead to major corrections with significant uncertainties for highly absorbed X-rays. The final term in the integral of the bulk $\phi(\rho z)$ model is uncertainty in the integral of the bulk $\phi(\rho z)$ model. This is difficult to characterize as most often this integral comes into play as part of a ratio of the $\phi(\rho z)$ -curve for two bulk materials. Thus the integral could be scaled by a constant factor but remain viable for use with bulk measurements. We know that this constant factor must be small since analytical $\phi(\rho z)$ models tend to agree with both measured $\phi(\rho z)$ curves and Monte Carlo simulated $\phi(\rho z)$ curves. We hypothesize that this may result in uncertainties of a few percent that would primarily impact the thickness measurement but this assumption requires experimental validation.

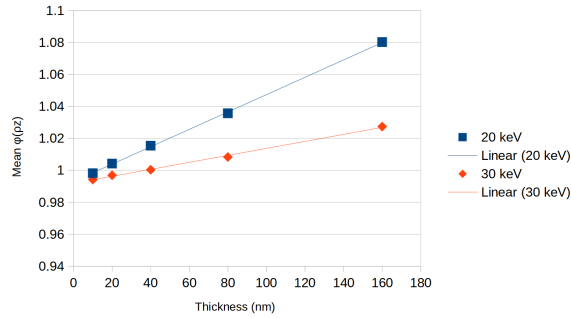


Figure 3: The mean $\phi(\rho z)$ over the depth of the thin film for thicknesses from 10 nm to 160 nm derived from Monte Carlo simulations of SiO₂ (density = 2.65 g/cm^3). The benefit of using higher incident beam energies is evident.

<i>Oxygen</i>	<i>Coated</i>	E_0	<i>Thickness</i>	<i>O</i>	<i>Mg</i>	<i>Si</i>	<i>Ca</i>	<i>Fe</i>
Measured	Carbon	20	76.8(74)	48.9(2)	7.4(1)	22.8(1)	11.4(1)	9.5(2)
Measured	Carbon	25	75.2(73)	48.9(2)	7.6(1)	22.7(2)	11.2(1)	9.6
Measured	Carbon	30	73.0(71)	48.1(2)	7.7(1)	22.8(1)	11.6(1)	9.8
Stoichiometry	Carbon	20	69.1(67)	42.8(1)	8.4(1)	25.6(1)	12.7(1)	10.6(2)
Stoichiometry	Carbon	25	67.5(65)	42.7	8.6(1)	25.5(1)	12.4(1)	10.7(1)
Stoichiometry	Carbon	30	66.4(64)	42.6	8.6(1)	25.3(1)	12.7(1)	10.8(1)
Measured	None	20	75.1(73)	47.8(2)	7.5(1)	23.3(1)	11.6(1)	9.8(2)
Measured	None	25	73.5(71)	47.9(2)	7.7(1)	23.1(2)	11.4(1)	9.9(1)
Measured	None	30	71.5(69)	47.1(2)	7.8(1)	23.2(1)	11.8(1)	10.0(1)
Stoichiometry	None	20	68.3(66)	42.7(1)	8.2(1)	25.5(1)	12.8(1)	10.7(2)
Stoichiometry	None	25	66.8(65)	42.7	8.5(1)	25.4(1)	12.6(1)	10.8(1)
Stoichiometry	None	30	65.7(64)	42.6	8.5(1)	25.2(1)	12.8(1)	10.9(1)
		Nominal	76(3)	43.30(160)	8.00(34)	25.40(98)	11.80(37)	11.10(88)

Table 3: The measured thickness and composition of a sample of SRM-2063a(Reed, 1993). The uncertainties on the measured thicknesses are due to the uncertainty in the glass density ($3.1(3) \text{ g/cm}^3$) The Nominal row represents the values published by NIST in the SRM-2063a certificate. The certificate certifies the composition and associated uncertainties but the thickness is only an informational value. Both are 95 % confidence intervals. Since the thickness in the SRM certificate is only an informational value, we validated the value using an electron energy loss measurement as reported in Table 4 and discussed in Appendix A. The Oxygen column indicates whether oxygen was measured directly or computed using stoichiometric assumptions. The Coating column indicates whether the sample was considered as one layer of SRM-2063a or as a layer of carbon on the surface of the SRM-2063a. The E_0 column represents the beam energy at which the data (unknown and standards) were collected.

3 Model Validation

3.1 Experimental Validation

There are few examples of available, well-characterized, multi-element thin films of known thickness. NIST developed SRM-2063 and SRM-2063a(Reed, 1993) to fill this void, however, neither is currently available for purchase. For the present analysis, we were able to access an instance of the SRM from a NIST archive.

A sample of SRM-2063a mounted on a TEM grid was analyzed in a TESCAN MIRA3 Schottky field-emission SEM with four EDAX silicon drift detectors with silicon nitride windows. The sample was mounted in a TESCAN STEM adapter with a TEM grid holder above a bright-field and a pair of dark-field detectors. The spectra were collected under automation using the SEMantics extension to NIST DTSA-II(Ritchie & Filip, 2011). Since it was not feasible to mount a Faraday cup on the STEM adapter, a piece of Cu was mounted on the STEM adapter and a copper spectrum was used as a proxy for a beam current measurement. A similar piece of copper was mounted on the standard block and the ratio of the number of counts in the $K\alpha$ peaks was used to compensate for differences

This paper 20 keV	23.8(2) $\mu\text{g/cm}^2$
This paper 25 keV	23.3(1) $\mu\text{g/cm}^2$
This paper 30 keV	22.6(1) $\mu\text{g/cm}^2$
Certificate	23.6(25) $\mu\text{g/cm}^2$
EELS (Kramers-Kronig)	27.6(3) $\mu\text{g/cm}^2$
EELS (log-ratio)	23.1(3) $\mu\text{g/cm}^2$

Table 4: Comparing the mass-thicknesses of SRM-2063a measured using Eqn 23 with the informational value in the SRM-2063a certificate(Reed, 1993) and electron energy loss spectroscopy (EELS) measurements described in Appendix A. The uncertainties are only those due to the scatter in the data over multiple measurements. The uncertainties do not reflect model-based inaccuracies which are likely to be on the order of 10%.

<i>Element</i>	<i>Z</i>	<i>Normalized</i>		
		<i>Mass Fraction</i>	<i>Mass Fraction</i>	<i>Atom Fraction</i>
Oxygen	8	0.3398	0.3413	0.6223
Aluminum	13	0.0664	0.0667	0.0721
Silicon	14	0.0405	0.0407	0.0423
Calcium	20	0.0683	0.0686	0.0499
Titanium	22	0.0713	0.0716	0.0436
Zinc	30	0.1055	0.1060	0.0473
Germanium	32	0.3037	0.3051	0.1225
	19.9666	0.9955	1.0000	1.0000

Table 5: ADM-6005a glass, assumed density 4 g/cm³

in probe current. Five spectra each were collected at 20 kV, 25 kV, and 30 kV.

The resulting spectra were processed in four permutations of the options 1) measuring oxygen or computing oxygen by stoichiometry; 2) assuming a top layer of carbon over the glass or as a single layer of glass. The results are presented in Table 3. All of the results in which we measure oxygen directly overestimate the oxygen content. We suspect this is because there is additional oxygen contamination on the surface of the sample or in the conductive carbon coating. Because of normalization, this forces the other elemental mass-fractions down. However, when we use stoichiometry to estimate the oxygen content ($Mg \mapsto MgO$, $Si \mapsto SiO_2$, $Ca \mapsto CaO$, $Fe \mapsto FeO$) we get both a more reasonable estimate of oxygen content and better accuracy in the other elements. Whether we assumed there was a carbon coating on the surface of the glass had negligible influence on the measured composition and thickness particularly when oxygen was computed by stoichiometry.

On the other hand, the thickness measurements are closer to the information value in the SRM certificate for the measured oxygen than for the computed oxygen. Regardless, the uncertainty in the measured thickness is large due to uncertainties in both the nominal value (76(3) nm) and the nominal density (3.1(3) g/cm³).

3.2 Monte Carlo Validation

We also validated Eq. 20 using Monte Carlo simulation. While experimental validation is typically preferable, Monte Carlo modeling does offer certain advantages. For one, it is possible to know precisely the composition and thickness of the film since they are model parameters. The underlying models for the $\phi(\rho z)$ and Monte Carlo models are very different. $\phi(\rho z)$ models are analytical expressions representing the depth distribution of ionizations. Monte Carlo models implicitly generate a similar depth distribution but use Mott elastic scattering cross-sections (Jablonski et al., 2010), Bethe energy loss (Bote & Salvat, 2008) and randomized electron trajectory modeling. Both types of models do share identical mass-absorption coefficients (Chantler et al., 2005) but otherwise they represent very different approaches to the same problem.

We simulated measurements at 30 keV using a typical EDS detector with take-off angle of 40° of films of 1 nm, 2 nm, 5 nm, 10 nm, 20 nm, 35 nm, 50 nm, 100 nm, 150 nm, 200 nm, 250 nm, and 300 nm thickness of ADM-6005a glass the details of which are provided Table 5. In addition, we simulated spectra for use as standards from bulk instances of SiO₂, Al, CaF₂, Ti, Zn and Ge using the same beam energy and detector configuration.

The simulated bulk spectra were fit to the simulated film spectra to extract k-ratios. The K-lines of each element were used to quantify the films using Eq. 20. The results are presented in Table 6.

A second example demonstrates the technique for two layers. The top layer is assumed to be Al₂O₃ and the lower layer is CaF₂. We used bulk MgO, Al, CaCO₃ and NaF as standards. We simulated a range of thicknesses from 10 nm to 100 nm for each layer. The results are presented in Table 7.

4 Discussion

As equation Eq. 18 suggests, the technique presented here breaks the problem into two parts - the composition and a scale factor proportional to the mass-thickness. These two parts are informed by the intensity data which is derived from measurements of pure and simple bulk compounds. The

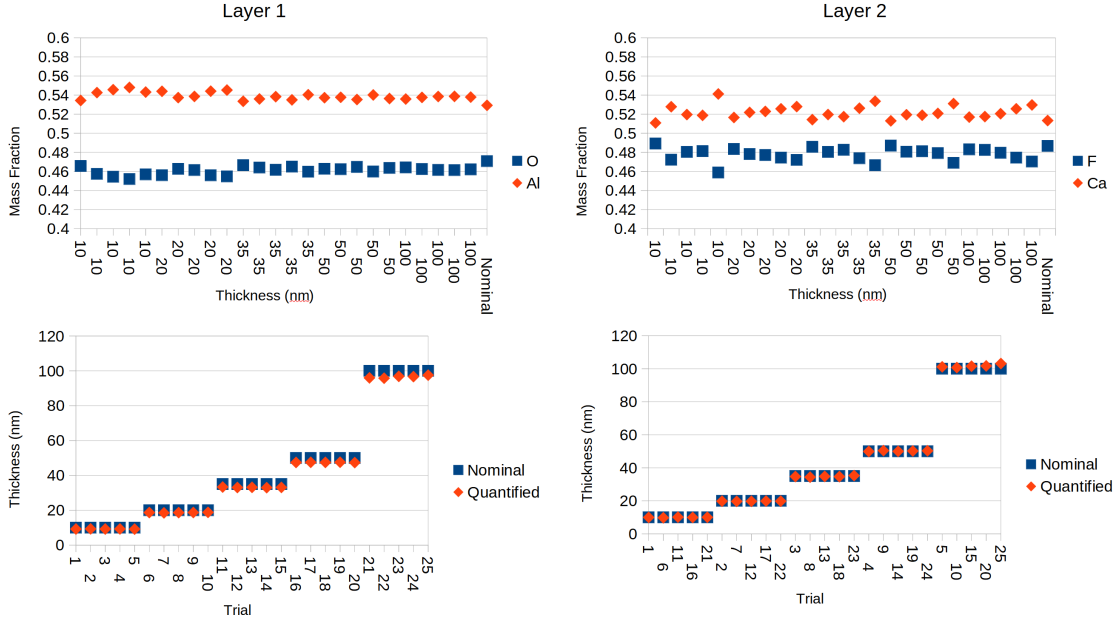


Figure 4: Plots of the results in Table 7. The top plot compares the quantified mass-fraction of each element with the nominal value (right-most point.) The bottom plot compares the nominal modeled thickness with the thickness quantified from the spectra via Eq. 23. There does not seem to be a distinct trend in the mass-fraction data for layer 1 however the O number is consistently underestimated and the Al number is consistently overestimated. Layer 2 shows a series of cycles that are a result of changes in thickness in layer 1. The estimated mass-fraction is best in layer 2 when layer 1 is the thinnest.

model builds on well established $\phi(\rho z)$ algorithms used in bulk analysis but is particularly dependent the integral of the absorption corrected $\phi(\rho z)$ curve (Eq. 11). Some authors have chosen to make this integral a fundamental defining characteristic of their $\phi(\rho z)$ models. This makes these models suitable for both simulating bulk spectra and for performing thin-film quantification.

Samples with mass thickness less than approximately $100 \mu\text{g}/\text{cm}^2$ are suitable for analyses at a beam energy of 30 keV. At lower beam energies, the suitable range will scale approximately as $(E_0/30.0)^{1.6}$ where E_0 is in kilo-electronvolts.

Using the same detector and sample geometry to collect the spectra from the thin film and standards brings many benefits including eliminating the need to know detector solid angle, detector efficiency, ionization cross-sections and fluorescence yields. The measurement is reduced to determining the ratio of a pair of measured intensities. This process we have decades of experience with as is discussed below.

A consistent geometry can be maintained by 1) performing the analysis on the optic axis; 2) using the same working distance; and 3) maintaining the detector position. Neither the sample nor standards should be tilted as is sometimes done in STEM to enhance X-ray generation as the absorption correction assumes normal incidence. Extending the technique to non-normal incidence should be straightforward.

This technique can also make use of the shape information present in the bulk spectra to deconvolve the spectra collected from the unsupported thin films thus resolving the issue of peak interferences. Because the filter-fit technique (Schamber, 1977) does not require an explicit continuum model, it is suitable for taking spectra collected on bulk materials and applying them to spectra collected on unsupported thin-films. It is not necessary to model either the bulk or thin-film continuum. The characteristic peak shape information which is almost identical between bulk and thin film is retained so that it is possible to deconvolve elements in which the characteristic peak profiles interfere. The ideal standard materials for this technique are those in which the element's characteristic peaks do not interfere with the characteristic peaks from any other elements in the material. Thus pure elements or simple compounds are often good choices. However, this is not strictly necessary if additional

peak-shape reference spectra are used to deconvolve interferences in the standard spectra.

What makes this technique unique and particularly use-able is the way it pulls together multiple different pieces into a coherent whole which provides peak deconvolution, k-ratio extraction, k-ratio calibration, matrix correction and thickness measurement. There are a handful of techniques which can provide one or more of these capabilities. However, we are not aware of any other technique which brings together all these abilities. The result is a technique that can be implemented in a user-friendly manner in which spectra are the inputs and the output is a measure of composition and mass-thickness.

The technique has been implemented in NIST DTSA-II and is available starting with the Neptune release. NIST DTSA-II is available at <https://cstl.nist.gov/div837/837.02/epq/dtsa2/index.html> and the source code is available from <https://github.com/usnistgov/DTSA-II> and quantitative X-ray microanalysis library on which it depends is available from <https://github.com/usnistgov/EPQht>

X-rays generated from the grid or chamber by scattered electrons often contribute to the measured signal. So long as these X-rays represent elements not present in the sample, they can be neglected. They represent additional spurious signal but will not otherwise diminish or enhance the desired signal. If they interfere with X-ray lines from measured elements, the scattered X-rays can be fitted using bulk spectra and the resulting k-ratio discarded before the quantification process.

NIST SRM-2063 and SRM-2063a, which are no longer available but remain in demand, filled a metrological need for standards for the Cliff and Lorimer method. While it only provided a handful of elements, these data points were interpolated to provide a more complete set of elements. This interpolation however introduced additional uncertainties into compositional measurements. It would be better to have multiple standards which covered all elements of metrological interest.

The ζ -factor method also depends upon well-characterized standards. For pure elements, this means constructing thin-films of the pure element and measuring the thickness. The technique we propose could be useful for measuring the mass-thickness. For compound thin-film standards, our technique could be useful for both establishing the nominal composition and mass-thickness of the standard. As is often the case, it can be difficult to translate mass-thickness into thicknesses for thin-films because the density of deposited thin films can differ from their bulk counterparts.

Finally, we hope this technique will offer a practical method for the community to characterize standards for use in both Cliff and Lorimer and ζ -factor quantification.

Thickness (nm)	Measured (nm)	O	Al	Si	Ca	Ti	Zn	Ge
1	0.946	0.3338	0.0678	0.0327	0.0694	0.0683	0.0954	0.3326
2	2.01	0.3181	0.0601	0.0402	0.0755	0.0605	0.1029	0.3427
5	4.92	0.3267	0.0671	0.0405	0.0648	0.0747	0.1003	0.3258
10	10.04	0.3137	0.0637	0.0409	0.0681	0.0734	0.1078	0.3323
20	19.63	0.3186	0.0664	0.0403	0.0687	0.0755	0.1178	0.3126
35	35.42	0.3123	0.0672	0.0390	0.0679	0.0728	0.1117	0.3291
50	50.40	0.3213	0.0648	0.0414	0.0668	0.0726	0.1100	0.3231
100	103.3	0.3180	0.0669	0.0391	0.0681	0.0736	0.1109	0.3233
200	217.2	0.3191	0.0658	0.0400	0.0698	0.0739	0.1119	0.3195
250	279.9	0.3227	0.0671	0.0395	0.0679	0.0732	0.1118	0.3178
300	348.4	0.3254	0.0665	0.0402	0.0676	0.0740	0.1106	0.3157
Nominal	-	0.3398	0.0664	0.0405	0.0683	0.0713	0.1055	0.3037

Table 6: The thickness and mass-fraction estimates for each element from quantifying Monte Carlo thin-film spectra using Eq. 20. The first column is the nominal thickness and the second is the measured thickness.

Layer 1				Layer 2			
Nominal (nm)	Quantified (nm)	O	Al	Quantified (nm)	Thickness (nm)	F	Ca
10	9.24	0.466	0.534	10	9.97	0.489	0.511
10	9.32	0.457	0.543	20	19.8	0.483	0.517
10	9.26	0.454	0.546	35	34.7	0.486	0.514
10	9.27	0.452	0.548	50	49.9	0.487	0.513
10	9.16	0.457	0.543	100	101.2	0.483	0.517
20	18.7	0.456	0.544	10	9.76	0.472	0.528
20	18.5	0.463	0.537	20	19.7	0.478	0.522
20	18.7	0.461	0.539	35	34.4	0.480	0.520
20	18.7	0.456	0.544	50	50.4	0.481	0.519
20	18.8	0.455	0.545	100	100.7	0.483	0.517
35	33.3	0.467	0.533	10	10.13	0.480	0.520
35	33.1	0.464	0.536	20	19.8	0.477	0.523
35	33.2	0.462	0.538	35	34.8	0.483	0.517
35	33.0	0.465	0.535	50	50.0	0.481	0.519
35	33.1	0.460	0.540	100	101.5	0.479	0.521
50	47.4	0.463	0.537	10	9.94	0.481	0.519
50	47.5	0.462	0.538	20	19.9	0.474	0.526
50	47.5	0.465	0.535	35	34.7	0.474	0.526
50	47.6	0.460	0.540	50	50.2	0.479	0.521
50	47.3	0.464	0.536	100	101.7	0.474	0.526
100	96.0	0.464	0.536	10	10.07	0.459	0.541
100	95.8	0.462	0.538	20	19.8	0.472	0.528
100	96.9	0.461	0.539	35	35.3	0.466	0.534
100	96.7	0.461	0.539	50	50.3	0.469	0.531
100	97.5	0.462	0.538	100	103.2	0.470	0.530
Nominal		0.471	0.529	Nominal		0.487	0.513

Table 7: Tabulated results from quantifying simulated measurements of a layer of Al₂O₃ on a layer of CaF₂.

A EELS Thickness Measurements

The thickness of SRM-2063a is an informational value meaning that, unlike the compositional measures, it is not certified by NIST. For comparison, the thickness was also measured using two electron energy loss spectroscopy (EELS) techniques based on the Kramers-Kronig sum method(Iakoubovskii et al., 2008) and on the log-ratio method(Malis et al., 1988). Each of these techniques is estimated to have an accuracy of about 10%(Zhang et al., 2012). The measurements were taken on an FEI Titan 80-300 operating at 200 keV. The spectrometer was using a Gatan Tridiem imaging energy filter with spectral dispersion set to 200 meV. HyperSpy was used to determine the elastic scattering threshold using a 5 channel window to locate the inflection point in the spectral derivative(de la Peña et al., 2017, 2022). Hyperspy was also used to estimate the relative thickness (t/λ) using the log-ratio method. The thickness was then calculated using custom implementations of the above mentioned techniques. The measurement was repeated three times producing an average mass-thickness of 27.6(3) $\mu\text{g}/\text{cm}^2$ and 23.1(3) $\mu\text{g}/\text{cm}^2$ for the Kramers-Kronig and log-ratio techniques, respectively.

References

- BOLON, R., LIFSHIN, E. & CICCARELLI, M. (1975). Microanalysis of Thin Films and Fine Structure, J. Goldstein & J. Yakowitz (eds.), *Practical Scanning Electron Microscopy: Electron and Ion Microprobe Analysis*, 299–326, Springer.
- BOON, G. (2000). *Simultaneous Determination Of Specimen Composition And Thickness Using The Transmission Electron Microscope*, Ph.D. thesis, Chemical Engineering and Chemistry.
- BOON, G. & BASTIN, G. (2000). The Use of a ϕ (ρz) Model for Simultaneous Determination of Composition and Thickness in Analytical Transmission Electron Microscopy, *Ultramicroscopy* **85**, 1–7.
- BOON, G. & BASTIN, G. (2004). Quantitative Analysis of Thin Specimens in the TEM Using a ϕ (ρz)-Model, *Microchimica Acta* **147**, 125–133.
- BOTE, D. & SALVAT, F. (2008). Calculations of inner-shell ionization by electron impact with the distorted-wave and plane-wave born approximations, *Physical Review A* **77**, 042701.
- CASTAING, R. (1951). *Application des Sondes Électronique à une Méthode D’analyse Ponctuelle Chimique et Cristallographique*, Ph.D. thesis, University of Paris, publication ONERA No. 55 (1952).
- CHANTLER, C.T., OLSEN, K., DRAGOSET, R.A., CHANG, J., KISHORE, A.R., KOTCHIGOVA, S.A. & ZUCKER, D.S. (2005). X-Ray Form Factor, Attenuation and Scattering Tables, Tech. rep., National Institute of Standards and Technology, Gaithersburg, MD, URL <http://physics.nist.gov/ffast>, web Site: <http://physics.nist.gov/ffast> Available: 2007, May 1.
- CLIFF, G. & LORIMER, G.W. (1975). The Quantitative Analysis of Thin Specimens, *Journal of Microscopy* **103**, 203–207.
- DE LA PEÑA, F., OSTASEVICIUS, T., FAUSKE, V.T., BURDET, P., JOKUBAUSKAS, P., NORD, M., SARAHAN, M., PRESTAT, E., JOHNSTONE, D.N., TAILLON, J. ET AL. (2017). Electron Microscopy (Big and Small) Data Analysis with the Open Source Software Package HyperSpy, *Microscopy and Microanalysis* **23**, 214–215.
- DE LA PEÑA, F., PRESTAT, E., FAUSKE, V.T., BURDET, P., LÄHNEMANN, J., JOKUBAUSKAS, P., FURNIVAL, T., NORD, M., OSTASEVICIUS, T., MACARTHUR, K.E. & ET AL. (2022). hyper-spy/hyperspy: Release v1.7.3, Tech. rep., Zenodo, URL <https://zenodo.org/record/7263263>.
- DIJKSTRA, J.M., BASTIN, G.F., HEIJLIGERS, H.J. & KLEPPER, D. (1994). Quantitative EPMA and TEM of Unsupported Films, *Microchimica Acta* **114**, 277–284.
- DUNCUMB, P. (1968). EMMA, Combinaison D’un Microscope Electronique et D’Une Microsonde Electronique, *J Microsc* **7**, 581.
- FITZGERALD, R., KEIL, K. & HEINRICH, K.F.J. (1968). Solid-State Energy-Dispersion Spectrometer for Electron-Microprobe X-ray Analysis, *Science* **159**, 528–530, URL <http://science.sciencemag.org/content/159/3814/528>.
- GOLDSTEIN, J.I. (1979). Principles of Thin Film X-ray Microanalysis, J. Hren, J. Goldstein & D. Joy (eds.), *Introduction to Analytical Electron Microscopy*, 83–120, Springer.
- IAKOUBOVSKII, K., MITSUISHI, K., NAKAYAMA, Y. & FURUYA, K. (2008). Thickness Measurements With Electron Energy Loss Spectroscopy, *Microscopy Research and Technique* **71**, 626–631.
- JABLONSKI, A., SALVAT, F. & POWELL, C.J. (2010). NIST Electron Elastic-scattering Cross-section Database - SRD 64, Site: <https://www.nist.gov/document/srd64usersguidev3-2pdf>.
- JACOBS, M. (1973). Industrial Applications Of Analytical Electron Microscopy, *Journal of Microscopy* **99**, 165–175.

- JACOBS, M. & BABOROVSKA, J. (1972). Quantitative Microanalysis Of Thin Foils With A Combined Electron Microscope-Microanalyser (EMMA-3), *Electron Microscopy 1972* 136.
- LANG, C., HISCOCK, M., DAWSON, M. & HARTFIELD, C. (2014). Local thickness and composition analysis of TEM lamellae in the FIB, *Microelectronics Reliability* **54**, 1790–1793, URL <https://www.sciencedirect.com/science/article/pii/S002627141400239X>, sI: ESREF 2014.
- MACARTHUR, K.E., SLATER, T.J.A., HAIGH, S.J., OZKAYA, D., NELLIST, P.D. & LOZANO-PEREZ, S. (2016). Quantitative Energy-Dispersive X-Ray Analysis of Catalyst Nanoparticles Using a Partial Cross Section Approach, *Microscopy and Microanalysis* **22**, 71–81, URL <https://doi.org/10.1017/S1431927615015494>.
- MALIS, T., CHENG, S. & EGERTON, R. (1988). EELS Log-Ratio Technique For Specimen-Thickness Measurement in the TEM, *Journal of Electron Microscopy Technique* **8**, 193–200.
- MCCARTHY, J.J. & SCHAMBER, F.H. (1981). Least-Squares Fit with Digital Filter: A Status Report , K.F.J. Heinrich, D.E. Newbury & R.L. Mylebust (eds.), *Energy Dispersive X-Ray Spectrometry* , *NBS Special Publication*, vol. 604, 273–296, National Bureau of Standards.
- MOY, A. & FOURNELLE, J. (2020). BadgerFilm: An Open Source Thin Film Analysis Program, *Microscopy and Microanalysis* **26**, 496–498.
- NASIR, M. (1972). Quantitative Analysis on Thin Films in EMMA-4 Using Block Standards, *Electron Microscopy 1972* 142.
- NEWBURY, D.E. & RITCHIE, N.W.M. (2015). Performing Elemental Microanalysis with High Accuracy and High Precision by Scanning Electron Microscopy/Silicon Drift Detector Energy-Dispersive X-ray Spectrometry (SEM/SDD-EDS), *Journal of Materials Science* **50**, 493–518.
- PARISINI, A., FRABONI, S., GAZZADI, G.C., ROSA, R. & ARMIGLIATO, A. (2018). Comparison of Cliff–Lorimer-Based Methods of Scanning Transmission Electron Microscopy (STEM) Quantitative X-Ray Microanalysis for Application to Silicon Oxycarbides Thin Films, *Microscopy and Microanalysis* **24**, 193–206.
- PHILIBERT, J. & TIXIER, R. (1968). Electron Penetration and the Atomic Number Correction in Electron Probe Microanalysis, *Journal of Physics D: Applied Physics* **1**, 685, URL <https://iopscience.iop.org/article/10.1088/0022-3727/1/6/302>.
- POUCHOU, J.L. & PICOIR, F. (1991). Quantitative Analysis of Homogeneous or Stratified Microvolumes Applying the Model ‘PAP’, K. Heinrich & D. Newbury (eds.), *Electron Probe Quantitation*, 31–75, Springer, URL http://www.ebook.de/de/product/3835664/electron_probe_quantitation.html.
- REED, W.P. (1993). Standard Reference Material 2063a, SRM Certificate 2063a, National Institute of Standards and Technology, Gaithersburg, MD 20899, URL <https://archive.org/details/srm-2063a>.
- RITCHIE, N.W. (2020). Embracing Uncertainty: Modeling The Standard Uncertainty In Electron Probe Microanalysis — Part I, *Microscopy and Microanalysis* **26**, 469–483.
- RITCHIE, N.W.M. & FILIP, V. (2011). SEMantics for High Speed Automated Particle Analysis by SEM/EDX, *Microscopy and Microanalysis* **17**, 896.
- SCHAMBER, F.H. (1977). A Modification of the Linear Least-Squares Fitting Method Which Provides Continuum Suppression., T.G. Dzubay (ed.), *X-ray Fluorescence Analysis of Environmental Samples*, 241–257, Ann Arbor Science Publishers.
- STATHAM, P. (2018). Method for Measuring the Mass Thickness of a Target Sample for Electron Microscopy, US Patent 10,054,557.
- STATHAM, P., SAGAR, J., HOLLAND, J., PINARD, P. & LOZANO-PEREZ, S. (2018). A Convenient Method for X-ray Analysis in TEM that Measures Mass Thickness and Composition, *IOP Conference Series: Materials Science and Engineering* **304**, 012017, URL <https://dx.doi.org/10.1088/1757-899X/304/1/012017>.

- SWEENEY JR, W., SEEBOLD, R. & BIRKS, L. (1960). Electron Probe Measurements of Evaporated Metal Films, *Journal of Applied Physics* **31**, 1061–1064, URL <https://aip.scitation.org/doi/10.1063/1.1735746>.
- VARAMBHIA, A., JONES, L., LONDON, A.J., OZKAYA, D., NELLIST, P.D. & LOZANO-PEREZ, S. (2018). Determining eds and eels partial cross-sections from multiple calibration standards to accurately quantify bi-metallic nanoparticles using stem., *Micron* **113**, 69–82.
- WATANABE, M. & WILLIAMS, D. (2006). The Quantitative Analysis of Thin Specimens: A Review of Progress from the Cliff-Lorimer to the New ζ -factor Methods, *Journal of Microscopy-Oxford* **221**, 89–109.
- YAKOWITZ, H. & NEWBURY, D. (1976). Simple Analytical Method for Thin Film Analysis with Massive Pure Element Standards, *Scanning Electron Microscopy* 151–162.
- ZHANG, H.R., EGERTON, R.F. & MALAC, M. (2012). Local Thickness Measurement Through Scattering Contrast and Electron Energy-Loss Spectroscopy, *Micron* **43**, 8–15, URL <https://www.sciencedirect.com/science/article/pii/S0968432811001120>, applications of EELS in Materials and Physics Research.